Seasonal and diel modulation of DOM in a mangrove-dominated estuary

L.O. Vidal, T. Lambert, L.C. Cotovicz Jr., M.C. Bernardes, R. Sobrinho, F. Thompson, G.D. Garcia, B.A. Knoppers, P.V. Gatts, C.R. Régis, et al.

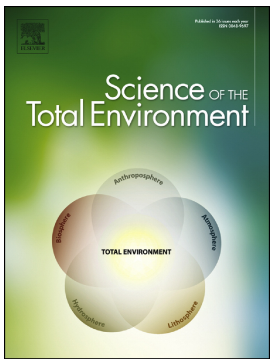

Seasonal and diel modulation of DOM in a mangrove-dominated estuary

L.O. Vidal, T. Lambert, L.C. Cotovicz Jr., M.C. Bernardes, R. Sobrinho, F. Thompson, G.D. Garcia, B.A. Knoppers, P.V. Gatts, C.R. Régis, G. Abril, C.E. Rezende

PII: S0048-9697(22)06144-7

DOI: https://doi.org/10.1016/j.scitotenv.2022.159045

Reference: STOTEN 159045

To appear in: *Science of the Total Environment*

Received date: 6 July 2022

Revised date: 7 September 2022

Accepted date: 22 September 2022

Please cite this article as: L.O. Vidal, T. Lambert, L.C. Cotovicz Jr., et al., Seasonal and diel modulation of DOM in a mangrove-dominated estuary, *Science of the Total Environment* (2022), https://doi.org/10.1016/j.scitotenv.2022.159045

Seasonal and diel modulation of DOM in a mangrove-dominated estuary

[1,2]Vidal, L.O*.; [3]Lambert, T.; [7,8]Cotovicz Jr., L.C.;[4]Bernardes, M.C.; [4]Sobrinho, R.; [5]Thompson, F.; [5]Garcia, G.D.;[4]Knoppers, B.A.;[1]Gatts, P.V.; [4]Régis, C. R.; [6]Abril, G.; [1]Rezende, C.E*.

[1] Laboratório de Ciências Ambientais, Centro de Biociências e Biotecnologia Universidade Estadual do Norte Fluminense, Campos dos Goytacazes, RJ, Brazil.

[2] Programa de Pós-graduação em Ecologia e Recursos Naturais, Universidade Estadual do Norte Fluminense, Campos dos Goytacazes, RJ, Brazil.

[3]Institute of Earth Surface Dynamics, University of Lausanne, Lausanne, Switzerland

[4] Programa de Geoquímica, Universidade Federal Fluminense, Niterói, RJ, Brazil

[5] Laboratório de Microbiologia, Centro de Ciências da Saúde, Universidade Federal do Rio de Janeiro.

[6] Laboratoire de Biologie des Organismes et Ecosystèmes Aquatiques (BOREA), UMR 8067, Muséum National d'Histoire Naturelle, CNRS, IRD, SU, UCN, UA, Paris, France.

[7] Department of Marine Chemistry, Leibniz Institute for Baltic Sea Research, Warnemunde, Germany.

[8] Instituto de Ciências do Mar, Universidade Federal do Ceará (UFC), Fortaleza, Brazil.

*Corresponding authors: Luciana O. Vidal, Email address: lovidal20@gmail.com; Carlos Eduardo de Rezende, Email address: crezende@uenf.br

Abstract

Rivers and estuaries are the main links between continents and oceans. The Paraíba do Sul River is among the most important rivers of the southeastern Brazilian region, carrying an average of 0.08 Tg of dissolved organic matter (DOM) to the ocean but has been facing significant changes in river discharge. In this study, we aimed to provide insights into the sources and transformations of chromophoric dissolved organic matter (CDOM) and fluorescent dissolved organic matter (FDOM) sources across a salinity gradient under changing river discharge scenarios. Three spatial surveys were performed covering the entire salinity gradient of the main estuarine channel and surrounding mangrove waters under contrasting river discharge (178 to 1,240 $m^3 s^{-1}$), and diel sampling was conducted in the mangrove tidal creek. The characterization of DOM through the parallel factor analysis (PARAFAC) model identified six components across the river-ocean gradient and mangrove creek: terrestrial origin (C1 - fulvic acid and C2 and C3 - humic-like), protein-like (C4), tryptophan-like (C5), and tyrosine-like (C6). Our results showed a shift in DOM composition and contribution along the salinity gradient, from terrestrial (C3) to autochthonous (C5 and C6) signatures. The October–17 dry campaign was characterized by a higher proportion of microbial protein-like component C4 and a lower contribution of humic-like components compared to February-17 and March-18 across the salinity gradient with an increase in the mixing zone. The DOM compositions of the February 17 dry and March 18 wet campaigns were similar. Additionally, the March–18 wet campaign, marked by the highest river discharge, showed higher inputs of terrestrial DOM (C1-C3 components) compared to February-17 in the estuary, which allowed DOM to be transported rather than transformed. The mangrove diel study showed that tidal fluctuations are also an important driver of carbon input to the mangrove creek with a possible impact on DOM composition in estuarine waters.

Keywords: tropical estuary, dissolved organic matter, CDOM; FDOM, PARAFAC, river-ocean gradient.

1. Introduction

Rivers and estuaries are the main link between continents and oceans, connecting more than 87% of Earth's surface to coastal regions (Hedges et al., 1997; Ludwig and Prosbst, 1998). Scientists have highlighted the important role of coastal ecosystems in the global carbon cycle, as well as their extreme sensitivity to local and global environmental changes such as eutrophication, ocean acidification, riverine flow regimes and sea level rise (Bianchi and Allison, 2009; Chilton et al., 2021). The continent-ocean interface receives large amounts of carbon and nutrients from river discharge and, to a lesser extent, carbon and nutrient inputs from marine sources, supporting high biological activity (Chen and Borges, 2009). In addition, mangrove-derived carbon is an important contributor to estuarine and coastal carbon pools (Dittmar et al., 2001; Dittmar et al., 2006; Rezende et al., 2007; Barroso-Matos et al., 2012; Cawley et al., 2014) and, together with riverine fluxes, provides the most important sources of terrigenous organic matter to the ocean (Dittmar et al., 2008). However, the dynamics of DOM composition in South Atlantic mangroves are unknown.

The use of optical indices has been successfully applied to assess the transformation of DOM in estuaries distributed worldwide (Helms et al., 2008; Huguet et al., 2009; Yang et al., 2013; Osburn et al., 2016). In general, the dissolved organic carbon (DOC) concentration shifts from high to low concentrations, and the fluorescence DOM characteristics shift from high molecular weight DOM to low molecular weight DOM between the upper and mid-estuary and finally to protein-like DOM in the lower estuary, reflecting an increase in the contribution of autochthonous DOM relative to terrigenous DOM closer to the estuary mouth (Yamashita et al., 2008; Fellman et al., 2011). These DOM transformations have been mainly associated with changes in a variety of biological, chemical, and physical processes (Medeiros et al., 2017) under different scenarios of river flow and salinity gradients (Fellman et al., 2011; Guo et al., 2011; Yang et al., 2013; Dixon et al., 2014; Jiang et al., 2016; Osterholz et al., 2016; Osburn et al., 2016; Yang et al., 2019).

River flows are predicted to experience an overall drying trend in midlatitude temperate regions and the wet–dry tropics, with a decrease in mean precipitation (Greve et al., 2018; Chilton et al., 2021). The Paraíba do Sul River, considered medium in size, has already suffered decrease the in precipitation levels (Cotovicz Jr. et al., 2020).

Estuaries located in low latitude regions receive approximately two-thirds of terrestrial organic carbon from rivers and have high rates of microbial decomposition due to high temperatures (Laws et al., 2000; Fuhrman et al., 2008), which makes the importance of those ecosystems to the global carbon cycle even more complex in the face of the already occurring changes in climate (IPCC, 2014).

In this study, we aimed to provide insights into the sources and transformations of chromophoric dissolved organic matter (CDOM) and fluorescent dissolved organic matter (FDOM) across a salinity gradient under changing river discharge scenarios, from low to high flow levels, and improve our understanding of the biogeochemical cycling of dissolved organic carbon delivery to the ocean by tropical estuaries in the face of global climate change. First, the spatial and temporal distributions of those DOM parameters were explored along a river-ocean salinity gradient under three contrasting hydrological conditions. Second, we conducted a diel study in the mangrove creek area to better understand the role of tidal inundation on the release of terrestrial mangrove DOM during high river discharge with possible implications for carbon delivery to the internal estuary and ultimately to the ocean.

2. Material and Methods

Study Site

The Paraiba do Sul River is an important water resource located in the southeastern region of Brazil. The river watershed presents an area of approximately 54,400 km^2, with a length of 1,145 km, traversing the most industrialized and urbanized region of Brazil (States of São Paulo, Minas Gerais and Rio de Janeiro). According to previous studies, the river basin can be divided into three regions (Ovalle et al., 2013): 1. The upper basin, with an area of 7,300 km^2, comprises its water sources at 1,800 m of altitude until 600 m in a valley of crystalline rocks; 2. The medium basin, with an area of 27,500 km^2 and an average elevation of 500 m; 3. The lower basin, with an area of 22,500 km^2, was occupied by coastal plains, with extensive meanders and islands, until the mouth into the Atlantic Ocean (Figure 1a).

The Paraiba do Sul River Estuary (PSRE) is located in the northern region of Rio de Janeiro State (Lat. 21°37′S, Long. 41°01′W), composed of a main river channel

and a minor secondary channel (Figure 1b). The secondary channel harbors a mangrove forest with a superficial area of approximately 8 km^2 (Sterza and Fernandes, 2006). The coast presents microtidal characteristics, with high wave energy, forming an estuarine delta. The weather in the region, according to the Köppen scale, is classified as Aw type, with a wet summer period (November to January) and a dry winter (July to September) (Cotovicz Jr. et al., 2013). The river water discharge in the estuary follows the climatic characteristics, where the summer/early spring is characterized by high water flow, and the winter/early autumn is the period of low water flow, with discharges averaging 1158 $m^3 s^{-1}$ and 444 $m^3 s^{-1}$, respectively. The intensity of river discharge modulates the extension of the river plume in the adjacent coastal ocean (Ruddorff et al., 2011) and the residence time of waters in the mixing zone (Souza et al., 2010). During low river water discharge, the plume is reduced, and the river water takes approximately 10 days to reach the open ocean (salinity 35), whereas under high river flow, the plume is extended along the shelf, and the residence time decreases to 6 days (Souza et al., 2010).

The river has been suffering from increasing anthropogenic influences. The total human population was estimated to be approximately 5 million inhabitants in the watershed. Considering only the estuarine region, the surrounding population was estimated to be approximately 600,000 inhabitants (IBGE, 2018). In addition, the lower basin presents extensive farming, particularly sugar cane production (Ovalle et al., 2013). The coverage of wastewater treatment plans was still very low in the region, covering less than 50% of the total households. Consequently, the estuary receives large amounts of industrial, agricultural and domestic effluents, with high inputs of nutrients to the waters, shifting the ecosystem from oligotrophic to mesotrophic characteristics (Cotovicz Jr. et al., 2013). In addition, forty-seven reservoirs and hydroelectric dams were constructed along the drainage basin (Ovalle et al., 2013), changing the hydrological patterns in the river and potentially altering carbon cycling.

2.1 Sampling

Three spatial surveys were conducted in the estuary, including the months of February -17 (Feb.-17), October -17 (Oct.-17) and March -18 (Mar.-18). Samples were collected on Feb-17 (n = 17) and presented a monthly accumulated precipitation of 40 mm, which was 60 mm lower than the historical average, with a 7-day accumulated

precipitation before sampling of only 1 mm. The accumulated precipitation of only 1 mm over 7 days means that the rainfall was almost negligible in the week before the sampling campaign of Feb. -17. This was unexpected since February is historically considered part of the wet season (Fig. 1c). Sampling on Oct.-17 (n = 16) presented a monthly accumulated precipitation of 13 mm (80 mm lower than the historical average), with 7 days of accumulated precipitation before sampling of 4 mm. The month Mar.-18 presented a monthly accumulated precipitation of 376 mm, which was 267 mm lower than the historical data. In this way, the samplings during Feb. -17 and Oct.-17 can be considered dry conditions, and the sampling during Mar-18 can be considered wet conditions. These climatological characteristics influenced the hydrological pattern. The months of Feb.-17 and Oct.-17 presented low river discharge on the days of fieldwork, averaging 288 $m^3 s^{-1}$ and 178 $m^3 s^{-1}$, respectively (Figure 1c, d, Table 1). For the sampling days on Mar. -18 (n = 15), the river discharge averaged 1,240 $m^3 s^{-1}$. The mean historical river water discharge (reference period of 95 years, 1923-2018) presented higher values than the discharge on the days of sampling. The long-term trend in the historical data showed that the river discharge is decreasing at a rate of approximately 5 $m^3 s^{-1}$ per year, meaning that the mean discharge already decreased 475 $m^3 s^{-1}$ (Figure 1d). During the period of lowest freshwater discharge (Oct.-17), the mixing zone was located close to the river mouth, with an intrusion of brackish water (salinity ≤20) until approximately 4 km inside the internal estuary at high tide (Cotovicz Jr. et al., 2020). Consequently, at low river discharge, the river plume covered a small area (~30 km^2) in the adjacent shelf waters, with the marine zone (salinity > 30) located closest to the river mouth (between 3 and 6 km from the river mouth). In contrast, in Mar-18, the mixing zone was located outside the limit of the coast, and no salinity intrusion occurred in the internal estuary. During this high-flow period, the mixing zone covered the highest surface area (~63 km^2) in the adjacent shelf (extending to approximately 12 km from the river mouth), with the marine zone located far from the internal estuary (> 10 km).

During each sampling campaign, measurements of temperature, electrical conductivity, salinity, dissolved oxygen (DO), and pH in situ were performed with a multiparameter probe (YSI, Model 6600, Yellow Springs, Ohio, U.S.A.). Surface water was sampled in the mangrove creeks and in the main channel and plume offshore at discrete points distributed regularly along the whole salinity gradient (0 to 35). The spatial surveys covered the freshwater domain (upper estuary), the mixing zone

(complete salinity gradient) and the external estuary (river plume in the adjacent coastal ocean). Salinity was measured using the Practical Salinity Scale. Samples for chlorophyll *a* (Chl *a*), suspended particulate matter (SPM), nutrients, DOC, CDOM, and FDOM were also sampled for laboratory analyses as described below. The ancillary parameters were seasonally separated as follows: Feb.-17, Oct.-17 and Mar.-18. In addition, we separated the region of the mangrove creek from the main estuarine channel. In addition to the spatial study, a diel 21-hour water sampling every 3 hours was conducted in the Mar.-18 wet campaign in a mangrove tidal creek with low-salinity waters located in the secondary channel. The two ebb periods sampled during the mangrove diel variability showed different tidal amplitudes. The tidal amplitude of the first ebbing period was 0.42 m (from ~ 12:00 pm to 06:30 pm), and for the second ebbing, the amplitude was 0.64 m (from ~ 00:30 am to 09:30 am). In this way, we sampled one ebb tide in the daytime, followed by one flood tide at nighttime and one ebb tide at nighttime. For the first tidal cycle, the salinity did not present a significant difference between ebb and flood tides (Mann–Whitney Test; $p > 0.05$). However, the second ebb tide (nighttime) presented higher salinity values than the other sampled diurnal periods (Mann–Whitney Test; $p < 0.01$), following an atypical pattern. Daytime samples had a higher average temperature (30.0 ± 0.3 °C) than did nighttime samples (28.3 ± 0.3 °C).

2.2 Analytical methods

The concentration of DOC in filtered samples was determined by the high-temperature catalytic oxidation method on an automated TOC analyzer (Shimadzu TOC 5000) using five calibration solutions spanning the concentration range of the samples. All DOC data reported are the mean of three replicate injections, for which the coefficient of variance was <5%. Procedural blanks, including the filtration step, were obtained using ultrapure water. These blank samples did not contain any detectable amounts of DOC. The detection limit for DOC was 5 μM, and the analytical accuracy (relative to the reference material) and precision (replicate injections) were within ± 1 μM. The deep-sea reference material provided by D. Hansell (University of Miami, USA) was repeatedly analyzed in each run to control accuracy.

We determined the concentrations of ammonium ($NH4^+$), nitrate (NO_3^-), nitrite (NO_2^-), and phosphate PO_4^- in each sample by the colorimetric method as described in

Grasshoff et al. (1999). The dissolved inorganic nitrogen (DIN) was determined by the sum of $NH4^+$, NO_3^-, and NO_2^-. The water for Chl *a* was filtered with Whatman GF/F filters (precombusted at 500 °C for 6 hours). The filters were kept at −18 °C prior to analysis. Chl *a* was extracted from the filters with 90% acetone and quantified by spectrophotometry according to Strickland and Parsons (1972). The suspended particulate material (SPM) was determined by water filtration with Whatman GF/F filters (precombusted at 500 °C for 6 hours). The final concentration was determined by the filter weight difference before and after filtering divided by the sample volume filtered.

Absorbance was recorded on a Shimadzu 2700 UV/Vis spectrophotometer using a 1 cm quartz cuvette. Absorbance spectra were measured between 200 and 700 nm at 1 nm increments, and instrument noise was assessed by using ultrapure (Type 1) Milli-Q (Millipore) water as a blank. After subtracting the blank spectrum, the correction for scattering and index of refraction was performed by fitting the absorption spectra to the data over the 200–700 nm range according to the following equation:

$$A_\lambda = A_0 e^{-S(\lambda-\lambda 0)} + K \quad (A.1)$$

where A_λ and A_0 are the absorbance measured at defined wavelength λ and at reference wavelength λ_0 = 375 nm, respectively, S is the spectral slope (nm^{-1}) that describes the approximate exponential decline in absorption with increasing wavelength and K is a background offset. The fit was not used for any purpose other than to provide an offset value K that was then subtracted from the whole spectrum (Lambert et al., 2015).

Napierian absorption coefficients were calculated according to the following equation:

$$a_\lambda = 2.303 \times A_\lambda / L \quad (A.2)$$

where a_λ is the absorption coefficient (m^{-1}) at wavelength λ, A_λ is the absorbance corrected at wavelength λ and L is the path length of the optical cell in meters (0.01 m). Spectral slopes for the intervals 275–295 ($S_{275\text{-}295}$) nm and 350–400 ($S_{350\text{-}400}$) nm were determined from the linear regression of the log-transformed *a* spectra vs. wavelength. The slope ratio S_R was calculated as the ratio of ($S_{275\text{-}295}$) to ($S_{350\text{-}400}$) according to

Helms et al. (2008). S_R is related to the molecular weight distribution of DOM, with values less than 1 indicative of enrichment in high-molecular-weight compounds and high values above 1 indicative of a high degree of low-molecular-weight compounds (Helms et al., 2008). The a_{350} focused on absorption at 350 nm as a proxy for CDOM absorption.

Fluorescence intensity was recorded on a Perkin-Elmer LS55 fluorescence spectrometer using a 1 cm quartz cuvette across excitation wavelengths of 220–450 nm (5 nm increments) and emission wavelengths of 230–600 nm (5 nm increments) to build excitation–emission matrices (EEMs). If necessary, samples were diluted until A_{254} < 0.2 m^{-1} to avoid problematic inner filter effects (Ohno, 2002). Before each measurement session (i.e., each day), a Milli-Q water sample was also analyzed. EEM preprocessing, including removing first and second Raman scattering, standardization to Raman units, absorbance corrections and inner filter effects, was performed prior to PARAFAC modeling. The scans were standardized to Raman units (normalized to the integral of the Raman signal between 390 and 410 nm in emission at a fixed excitation of 350 nm) with a Milli-Q water sample run the same day as the samples (Zepp et al., 2004). The PARAFAC model was built using MATLAB (MathWorks, Natick, MA, USA) and DOM Fluorescence Toolbox 1.7. Validation of the PARAFAC model was performed by split-half analysis and random initialization (Stedmon and Bro, 2008). The maximum fluorescence F_{Max} values of each component for a particular sample provided by the model were summed to calculate the total fluorescence signal F_{Tot} of the sample in Raman units (RU). The relative abundance of any particular PARAFAC component X was then calculated as $\%C_X = F_{Max}(X)/F_{Tot}$. The humification index (HIX) is an indicator of humic substance content and was calculated as the ratio of the area under the emission spectra between 436-480 nm by the area between 300-346 nm at an excitation of 250 nm (Ohno, 2002). Commonly, higher values indicate an increase in the degree of humification.

The DOM components derived from PARAFAC modeling were compared with PARAFAC components from other studies through the OpenFluor database (Murphy et al., 2013). The complete absorption and emission spectra of the fluorescent components derived from PARAFAC are available in the OpenFluor database after publication (http://www.openfluor. org).

2.3 Statistics

We applied the Shapiro–Wilk test to investigate the normality of the dataset. As the data did not follow normal distributions, we applied nonparametric statistics. Kruskal–Wallis followed by post hoc Dunn's test to investigate seasonal variation for selected parameters. All statistical analyses were based on $\alpha = 0.05$. The statistical tests and calculations were performed with the SigmaPlot 12.5 program.

Principal component analysis (PCA) was performed to investigate the spatial and temporal changes in DOM sources. DOC concentrations, DOM composition including the relative contribution of PARAFAC components, S_R and HIX values, Chl *a*, salinity, PO_4 and DIN were used as the variables. Given the different variable units, data were scaled to zero mean and unit variance as recommended by Borcard et al. (2011). PCA was performed using the *prcomp* function in R software and the *factoextra* package was used to identify the variables that contributed the most to the first two dimensions of the PCA.

3. Results

3.1 Temporal and spatial variability in water quality, DOC concentration, composition, and optical properties

The water quality parameters showed marked seasonal variation (Table 1). The months of summer (Feb.-17 and Mar.-18) presented higher water temperatures, ranging between 26.2 °C and 31.6 °C (average 29.4 ± 0.5 °C). The winter period, in turn, represented by the campaign in Oct.-7, presented lower temperatures, ranging between 23.55 °C and 25.9 °C (average of 25.2 ± 0.74 °C). The salinity levels, in addition to the similar seasonal range and standard deviation values, showed the highest average value during the second dry campaign (Oct.-17). The second dry campaign (Oct.-17) and the wet campaign (Mar.-18) presented higher SPM average values than Feb.-17. However, the highest maximum value was presented by the second dry campaign (Oct.-17). The first dry campaign (Feb.-17) showed the highest average and maximum Chl a levels, and the wet campaign (Mar.-18) showed the lowest.

The average and standard deviation for DOC (mg L^{-1}), S_R, a_{350} (m^{-1}) and HIX separated by sampling campaigns and estuarine zones are presented in Table 2. In general, the DOC ranged from 1.40 ± 0.10 to 3.51 ± 0.16 mg L^{-1} for the Feb.-17

campaign, from 1.39 ± 0.20 to 2.99 ± 0.48 mg L^{-1} for the Oct.-17 campaign and from 1.28 to 12.91 ± 2.78 mg L^{-1} for the Mar.-18 campaign. The S_R ranged from 0.93 ± 0.26 to 2.14 ± 0.25 for the Feb.-17 campaign, from 0.80 ± 0.19 to 1.47 ± 0.28 for the Oct.-17 campaign and from 0.63 ± 0.04 to 1.65 for the Mar.-18 campaign. The a_{350} ranged from 1.04 ± 1.14 to 15.75 ± 1.42 m^{-1} for the Feb.-17 campaign, from 2.68 ± 0.51 to 10.88 ± 4.29 m^{-1} for the Oct.-17 campaign and from 0.92 to 53.89 ± 6.51 m^{-1} for the Mar.-18 campaign. The HIX ranged from 0.70 ± 0.11 to 0.90 ± 0.03 for the Feb.-17 campaign, from 0.10 ± 0.07 to 0.80 ± 0.06 for the Oct.-17 campaign and from 0.74 to 0.89 ± 0.07 for the Mar.-18 campaign. The longitudinal variability in DOC, S_R, a_{350} and HIX proxies showed seasonal variations with a tendency to decrease or increase across the salinity gradient (Figure 2).

3.2 PARAFAC modeling and principal component analyses

Six PARAFAC components were determined (Figure 3, Table 3) to adequately model our dataset, all of which have already been described in previous studies (Stedmon and Markager, 2005; Stedmon et al., 2007; Walker et al., 2009; Massicote and Frenette, 2011; Osburn et al., 2016; Asmala et al., 2018). Components included one fulvic-like fluorophore (C1), two humic-like fluorophores (C2 and C3), one microbial protein-like fluorophore (C4), and tryptophane (C5) and tyrosine (C6) protein-like fluorophores. Each component contribution (F_{Max} and %) for the sampled periods is listed in Table 2.

The first two components of the PCA explained 55.6% of the variance (Figure 4). Sampling locations and campaigns were used as descriptive variables in the PCA biplots (Figure 4-A and 4-B, respectively). The first principal component (PC1) was related to protein-like components C5 and C6, S_R and salinity (positive scores) and to DOC, humic-like C3 component and HIX values (negative scores). The second principal component (PC2) was related to the protein-like C4 component (positive scores) and to the humic-like C1 and C2 components (negative scores).

There was a shift in the dominant DOM composition along the salinity gradient during all campaigns (Figure 2, Figure 4-A), from terrestrial (DOC, C3) to autochthonous (C5 and C6) signatures, in parallel with a decrease in the average molecular weight of DOM (Figure 4-B) and an enrichment in protein-like components C5 and C6. The relative contribution of PARAFAC components across seasons

revealed by the PCA showed that DOM composition was similar in Feb.-17 and Mar.-18, with dominance of terrestrial humic-like components (C1-C3) but with higher inputs (F_{Max} values) during Mar.-18 (Table 2, Figure 5). On Oct.-17, DOM was enriched in microbial-like component C4 (and protein-like (C5-C6) tended to increase) but depleted in C1 and C2 humic-like components (Table 2, Figure 5) relative to summer seasons. A decrease in the humic-like (C3) component contribution during Oct.-17 (Figure 5) was also noticed.

3.3 Diel cycle reveals high DOM at the end of the tidal daytime

The results of the diurnal variations in salinity, depth and F_{Max} for each component are presented in Figure 6. As a direct consequence of the diel variation in F_{max} of PARAFAC components, the relative contribution of each component to the total fluorescence signal (F_{tot}) showed distinct diel variability (Figure 6). In general, the highest signals were registered at the end of ebb tide during daytime and in the middle of ebb tide during nighttime, following the salinity levels for all DOM components with the exception of the C6 tyrosine-like component, which showed the first peak in the beginning of ebb tidal daytime. Additionally, the lowest tidal height was coincident with the highest F_{max} for all the identified components.

4. Discussion

The relationship between the optical properties of dissolved organic matter (CDOM and FDOM) across salinity gradients has been assessed to show how DOM component diversity shifts from river to ocean depending on the contribution of organic components (Huguet et al., 2009; Fellman et al., 2011; Medeiros et al., 2017; Seidel et al., 2015; Gonçalves-Araújo, 2015). In general, it reflects the increased contribution of aquatic DOM relative to terrigenous DOM closer to the estuary mouth and in shelf waters. This trend was also observed in the present study. The results of this study showed a clear shift in DOM composition along the salinity gradient for all sampled periods characterized by decrease in the contribution of terrestrial DOM (C1 to C3 components) and an increase in autochthonous DOM (C5 and C6 components) from river/mangrove tidal creek waters to ocean waters (Table 2, Figures 4-B and 5). The spatial distribution of DOM may be explained by the combination of several processes,

including microbial- and photodegradation processes, flocculation, dilution, and aquatic production (Asmala et al., 2014; Moran and Zepp, 1997; Raymond and Bauer, 2000). However, in the present study, it was difficult to discuss the relative importance of each of these processes based on PARAFAC components without additional experiments. Overall, regardless of the dominant processes, it resulted in a decrease in the average molecular weight of DOM, also attested by increase in S_R and decrease in a_{350} values (Table 2, Figure 2).

Despite very contrasting river discharges, the PCA analysis (Figure 4B) and HIX values (Table 2, Figure 2) showed that the DOM composition was similar in Feb.-17 and Mar.-18. Otherwise, the PCA clearly indicates that DOM in Oct.-17 was enriched in the microbial-like C4 component and depleted in the terrestrial humic-like C1, C2 and C3 components compared to Feb.-17 and Mar.-18 (Figure 4 and 5) across the salinity gradient. These findings showed a complex behavior to the relationship between temporal and spatial variability of DOM composition for similar river discharges in the PSRE. Despite the contrasting changes in DOM, driven by the magnitude of river discharge, it is also important to consider the seasonality driven by temperature (Table 1), which may lead to higher metabolic activity and organic matter degradation (Caffrey, 2003; Apple et al., 2006) regulating DOM composition in the Feb.-17 and Mar.-18 campaigns.

During the lower river discharge of the Oct.-17 campaign, the oceanic waters were able to enter upward in the estuary, as attested by the higher salinities up to the mixing zone. During this period, the mixing zone was located close to the river mouth, with an intrusion of brackish water (salinity ≤20) up to approximately 4 km inside the internal estuary at high tide (Cotovicz Jr. et al., 2020). At that time, DOM was still a mixture of terrestrial and algal-DOM in the river (similar S_R values compared to Feb.-17), even if terrestrial inputs were lower compared to Feb.-17. The most important change in Oct.-17 was the increase in F_{Max} values of C4 in the river and mixing zone (Table 2) and, to a lesser extent, also for C5 and C6 in relation to Feb.-17. The protein-like components C5 and C6 are associated with algal-DOM (Fellman et al., 2011; Ziervogel et al., 2016), and the C4 component was derived from bacterial activity (Fellman et al., 2010; Fellman et al., 2011; Lambert et al., 2022). One possible explanation is that the increase in salinity provoked osmotic stress in freshwater phytoplankton communities during Oct.-17 (Cloern, 1996; Lancelot and Muylaert,

2011), leading to the death and flushing of freshwater cells that in turn released large amounts of algal-DOM along the salinity gradient, as shown by the increase in C5 and C6 components (Table 2, Figure 5) in Oct.-17. As a result, DOM during Oct.-17 was fresher (lower HIX) compared to Feb.-17 (Table 3, Figure 3). Knowing the high lability of algal material, this freshly produced autochthonous DOM was quickly consumed by heterotrophic bacterial communities, as shown by the increase in C4 components. This observation is supported by Lambert et al. (2022), where C4 built on the degradation of algal-DOM was quickly consumed during incubations.

During Feb.-17 there were favorable conditions for freshwater phytoplankton production in the river, as shown by the higher average chlorophyll *a* values (Table 1), but this concentration showed a marked decline seaward due to changes in salinity conditions (Cotovicz Jr. et al., 2020). This increase in riverine phytoplankton activity during low flow conditions was expected and was previously observed in estuaries (Dixon et al., 2014; Bhattacharya and Osburn, 2017). These observations are also supported by previous studies in this area (Cotovicz Jr. et al., 2020; Marques et al., 2017), in which it was hypothesized that algae can be a significant source of DOM in freshwater, based on chlorophyll *a* and $\delta^{13}C$ values. Otherwise, during Feb.-17, a mixture between DOM terrestrial and aquatic sources (S_R values range from 0.75 to 1.01) was observed in the river and mangrove zones, and the autochthonous contribution seemed to increase in the mixing zone, as indicatedindicated by a sudden increase in S_R values (Table 2, Figure 2). We may assume that salinity would be the main driver of this seasonal DOM diversity shift across the estuary from the Feb.-17 to Oct.-17 dry campaigns as a result of the change in the balance between freshwater (changes in river discharge) and saltwater intrusion (sea level rise) (Regier et al., 2016) into the internal estuary.

The Mar.-18 campaign was marked by high inputs of terrestrial DOM in the estuary shown by higher DOC in the river, mixing zone and mangrove zones, low S_R values in the river (< 0.8), a_{350} typical of terrestrial DOM and high F_{Max} for C1-C3 components (Table 2), despite the lower river discharge during the wet season compared to the historical discharge measurements for the Paraíba do Sul River (Table 1, Figure 1). S_R values remained below 1 almost along the whole salinity gradient (Figure 3), and values > 1 were observed only in oceanic waters. Higher discharge means higher water velocity, a decrease in water residence time and therefore less time

for degradation/flocculation and the accumulation of terrestrial DOM in the estuary. Consequently, a reduction in water residence time alloweded terrestrial DOM (C1-C3) to be transported rather than transformed (Raymond et al., 2016; Bhattacharya and Osburn, 2021). Additionally, Mar.-18 was characterized by a reduction in the C4-C6 component contribution (Table 2, Figure 5) compared to Oct.-17. This pattern has been attributed to low phytoplankton abundance and productivity or increased phytoplankton cell dilution by terrestrial CDOM (Amon et al., 2001; Peierls et al., 2012; Søndergaard et al., 2000).

The mangrove creek DOM composition also showed diverse sources in the PSRE zones. However, the terrestrial DOM humic-like (C3) component was identified with a higher contribution to the DOM pool in the mangrove creek during the diel study, probably associated withto the mangrove vegetation origin. This component contributed to a higher proportion of the river and mangrove zones during the Mar.-18 campaign, indicating terrestrial MOD source exchange between the river channel and mangrove sites (Table 2). The C1-C2 river terrestrial components were also found in the mangrove creek, although in a smaller proportion than the C3 component (Figure 6). The protein-like C5 component also showed a significant contribution during the diel study, which might be associated with algal DOM supported by high mangrove creek chlorophyll *a* levels during a study conducted in the same area (Cotovicz Jr. et al., 2020). Additionally, during diel measurements, the salinity variability proved to be important considering the modulation of DOM in the PSRE mangrove creek (Figure 6). In addition to the PSRE, mangrove salinity during the sampling time was always less than 1 and followed an inverse trend with the tidal level, acting as an inverse mangrove tidal creek (Cotovicz Jr. et al., 2020). This is explained by tidal pumping, an important process of exchange at the soil–water interface acting as a source of DOM to the adjacent tidal creek (Maher et al., 2015). Other studies have shown contrasting behavior for mangrove systems where the highest FDOM values corresponded to the lowest salinity attributed to dilution with freshwater enriched in DOM (Dittmar and Lara, 2001; Cawley et al., 2014; Regier and Jaffé, 2016). Additionally, the tidal height diel variability was followed by the inverse F_{Max} DOM component patterns (Figure 6), as in previous studies. The tidal creek is also a source of dissolved inorganic carbon, which is a result of aerobic and anaerobic processes of OM degradation (Cotovicz Jr. et al., 2020). This increase in DOM after saltwater intrusion resulted in higher carbon loss

from the mangrove forest, indicating that it is an important process that regulateses the DOM dynamics in the PSRE.

5. Conclusions

In this study, we aimed to provide insights into the sources and transformations of optical properties of dissolved organic matter across a salinity gradient in a tropical coastal delta under changing river discharge scenarios, from low to high flow levels, and thus improve our understanding of the biogeochemical cycling of dissolved organic carbon delivery to the ocean by tropical estuaries in the face of global climate change. Our findings followed previous studies where DOC concentrations showed a progressive decrease from high (upper estuary) to low (mid-lower estuary) concentrations. The variations in DOM composition in the present study reflected both the dynamics of phytoplankton and terrestrial inputs (higher during the wet period) from both the watershed and mangrove forest. It was possible to observe two very contrasting patterns in terms of DOM quality for dry conditions (Feb.-17 and Oct.-18) and very similar patterns between the first dry and wet campaigns (Feb.-17 and Mar.-18). This showed that despite the changes in DOM driven by the magnitude of river discharge, the seasonality driven by temperature is also important in regulating DOM composition in the estuary. Additionally, this study also showed that the mangrove forest accounted for the larger proportion of the humic-like (C3**)** source in the mangrove creek during the diel measurements, which was also detected in all PSRE estuary zones, contributing to the seasonal and spatial DOM dynamics in the PSRE.

This study showed that changes in river discharge as a consequence of climate change will affect the DOM quality that is delivered to the ocean. Our results reinforced the importance of knowing DOM spatial and temporal variability, mainly concerning DOM diversity, to better understand carbon cycling in tropical estuaries in a scenario of climate change. This study is timely and relevant for future efforts aimed at predicting the future of coastal ecosystems in the context of the C cycle.

Acknowledgments

The authors are grateful for the support from the Laboratory of Environmental Sciences and to the Graduate Program in Ecology and Natural Resources of the State University of Norte Fluminense Darcy Ribeiro. Carlos E. Rezende thanks the financial

support of Conselho Nacional de Desenvolvimento Científico e Tecnológico (CNPq) (305217/2017-8) and FAPERJ: Fundação Carlos Chagas Filho de Amparo à Pesquisa do Estado do Rio de Janeiro – Brazil (E-26/200.893/2017 and 210.883/2016). Luciana O. Vidal the financial support of a postdoctoral researcher fellowship of the Foundation for the Coordination of Higher Education and Graduate Training (CAPES; proc No. 88882.314551/2019-01). Luiz C. Cotovicz Jr. thanks the financial support of a postdoctoral researcher of the FAPERJ (proc. No. E-26202.785/2016). This work also contributes to the French CNRS-INEE International Research Project VELITROP (Vulnerability of Tropical Coastal Ecosystems to Eutrophication).

References

Amon, R.M.W., Fitznar, H.P., Benner, R. 2001. Linkages among the bioreactivity, chemical composition, and diagenetic state of marine dissolved organic matter. Limnol. Oceanogr. 46, 287–297. https://doi.org/10.4319/lo.2001.46.2.0287.

Apple, J.K., del Giorgio, P.A., Kemp, W.M. 2006. Temperature regulation of bacterial production, respiration, and growth efficiency in a temperate salt-marsh estuary. Aquat. Microb. Ecol. 43, 243-254. https://doi.org/10.3354/ame043243.

Asmala, E., Haraguchi, L., Markager, S., Massicotte, P., Riemann, B., Staehr, P.A. Carstensen, J. 2018. Water column nutrient, chlorophyll and dissolved organic matter concentrations and dissolved organic carbon characteristics in Roskilde Fjord, Denmark. PANGAEA, https://doi.org/10.1594/PANGAEA.895734.

Asmala, E., Bowers, D.G., Autio, R., Kaartokallio, H., Thomas, D.N. 2014. Qualitative changes of riverine dissolved organic matter at low salinities due to flocculation. J. Geophys. Res. Biogeosci. 119,1919–1933. https://doi: 10.1002/2014jg002722.

Barroso-Matos, T., Bernini, E., Rezende, C.E. 2012. Decomposition of mangrove leaves in the estuary of Paraíba do Sul River Rio de Janeiro, Brazil. Lat. A m. J. Aquat. Res., 40(2), 398-407. https://doi:10.3856/vol40-issue2-fulltext-14.

Bhattacharya, R., Osburn, C.L. 2021. Chromophoric dissolved organic matter composition and load from a coastal river system under variable flow regimes. Sci. Total Environ. 760 (15), https://doi.org/10.1016/j.scitotenv. 2020.143414.

Bhattacharya, R., Osburn, C.L. 2017. Multivariate analyses of phytoplankton pigment fluorescence from a Freshwater River network. Environ. Sci. & Technol. 51, 6683–6690. https://doi.org/10.1021/acs.est.6b05880.

Bianchi, T., Allison, M. 2009. Large-river delta-front estuaries as natural "recorders'' of global environmental change. Proc. Natl. Acad. Sci. U.S.A. 106, 8085-92. https://doi.org/10.1073/pnas.0812878106.

Borcard, D., Gillet, F., Legendre, P. 2011. Numerical ecology with R, Springer New York, New York, 306 pp. https://doi.org/10.1007/978-1- 4419-7976-6.

Caffrey, J.M. 2003. Production, Respiration and Net Ecosystem Metabolism in U.S. Estuaries. Environ. Monit. Assess. 81**,** 207–219. https://doi.org/10.1023/A:1021385226315.

Cawley, K.M., Yamashita, Y., Maie, N., Jaffé, R. 2014. Using Optical Properties to Quantify Fringe Mangrove Inputs to the Dissolved Organic Matter (DOM) Pool in a Subtropical Estuary. Estuaries Coast, 37(2), 399–410. doi:10.1007/s12237-013-9681-5.

Chen, C.T.A., Borges, A.V. 2009. Reconciling opposing views on carbon cycling in the coastal ocean: continental shelves as sinks and near-shore ecosystems as sources of atmospheric CO2. Deep-Sea Res. II, 56 (8-10), 578-590. https://doi.org/10.1016/j.dsr2.2009.01.001.

Chilton, D., Hamilton, D.P., Nagelkerken, I., Cook, P., Hipsey, M.R., Reid, R., Sheaves, M., Waltham, N.J., Brookes, J. 2021. Environmental Flow Requirements of Estuaries: Providing Resilience to Current and Future Climate and Direct Anthropogenic Changes. Front. Environ. Sci. 9,764218. https:// 10.3389/fenvs.2021.764218.

Cloern, J.E. 1996. Phytoplankton bloom dynamics in coastal ecosystems: a review with some general lessons from sustained investigation of San Francisco Bay, California. Rev. Geophys. 2, 127–168. https://doi.org/10.1029/96RG00986.

Cotovicz Jr., L.C., Vidal, L.O., de Kerzende, C.E., Bernardes, M.C., Knoppers, B.A., Sobrinho, R.L., Cardoso, R.P., Muniz, M., dos Anjos, R.M., Biehler, A., Abril, G. 2020. Carbon dioxide sources and sinks in the delta of the Paraíba do Sul River (Southeastern Brazil) modulated by carbonate thermodynamics, gas exchange and ecosystem metabolism during estuarine mixing. Mar. Chem. 226,103869. https://doi.org/10.1016/j. marchem.2020.103869.

Cotovicz Jr., L.C., Brandini N., Knoppers B.A., Mizerkowski B.D., Sterza J.M., Ovalle A.R.C., Medeiros P.R.P. 2013. Assessment of the trophic status of four coastal lagoons and one estuarine delta, eastern Brazil. Environ. Monit. Assess. 185, 3297–3311. https://doi.org/10.1007/s10661-012-2791-x.

Dittmar, T., Koch, B., Hertkorn, N., Kattner, G. 2008. A simple and efficient method for the solid-phase extraction of dissolved organic matter (SPE-DOM) from seawater. Limnol. and Oceanogr. Methods. 6, 230–235. https://doi.org/10.4319/lom.2008.6.230.

Dittmar, T., Hertkon, N., Kattner, G., Lara, R.J. 2006. Mangroves, a major source of dissolved organic carbon to the oceans. Global Biogeochem. Cycles. 20, GB1012. https://doi.org/10. 1029/2005GB002570.

Dittmar, T., Lara, R.J., Kattner, G. 2001. River or mangrove? Tracing major organic matter sources in tropical Brazilian coastal waters. Mar. Chem. 73, 253–271. https://doi.org/10.1016/S0304-4203(00)00110-9.

Dixon, J.L., Osburn, C.L., Paerl, H.W., Peierls, B.L. 2014. Seasonal changes in estuarine dissolved organic matter due to variable flushing time and wind-driven mixing events. Estuar. Coast. Shelf Sci. 151, 210-220. https://doi.org/10.1016/j.ecss.2014.10.013.

Fellman, J.; Petrone, K.; Grierson, P. 2011. Source, biogeochemical cycling, and fluorescence characteristics of dissolved organic matter in an agro-urban estuary. Limnol. Oceanogr. 56, 243-256. https://doi.org/10.4319/lo.2011.56.1.0243.

Fellman, J.B., Hood, E. Spencer, R.G.M. 2010. Fluorescence spectroscopy opens new windows into dissolved organic matter dynamics in freshwater ecosystems: A review. Limnol. Oceanogr. 55, 2452–2462. https://doi:10.4319/lo.2010.55.6.2452.

Fuhrman, J.A., Steele, J.A., Hewson, I., Schwalbach, M.S., Brown, M.V., et al. 2008. A latitudinal diversity gradient in planktonic marine bacteria. Proc. Natl. Acad. Sci. U.S.A. 1005, 7774–7778. https://doi:10.1073/pnas.0803070105.

Gonçalves-Araujo, R., Stedmon, C.A., Heim, B., Dubinenkov, I., Kraberg, A., Moiseev, D., Bracher, A. 2015. From Fresh to Marine Waters: Characterization and Fate of Dissolved Organic Matter in the Lena River Delta Region, Siberia. Front. Mar. Sci. 2, 108. https://doi:10.3389/fmars.2015.00108.

Grasshoff, K., Ehrhardt, M., Kremling, K. 1999. Methods of Seawater Analysis, 3rd edition, Wiley-VCH, Weinhein.

Greve, P., Gudmundsson, L., Seneviratne, S. I. 2018. Regional Scaling of Annual Mean Precipitation and Water Availability with Global Temperature Change. Earth Syst. Dynam. 9 (1), 227–240. https://doi:10.5194/esd-9-227-2018.

Guo, W., Yang, L., Hong, H., Stedmon, C., Wang, F., Xu, J., Xie, Y. 2011. Assessing the dynamics of chromophoric dissolved organic matter in a subtropical estuary using parallel factor analysis. Mar. Chem. 124, 125-133. https://doi:10.1016/j.marchem.2011.01.003.

Hedges, J.I., Keil, R.G., Benner, R. 1997. What happens to terrestrial organic matter in the ocean? Org. Geochem. 27, 195–212. https://doi.org/10.1016/S0146-6380(97)00066-1.

Helms, J.R., Stubbins, A., Ritchie, J.D., Minor, E.C., Kieber, D.J., Mopper, K. 2008. Absorption spectral slopes and slope ratios as indicators of molecular weight, source, and photobleaching of chromophoric dissolved organic matter. Limnol. Oceanogr. 53, 955–969. https://doi.org/10.4319/lo.2008.53.3.0955.

Huguet, A., Vacher, L., Relexans, S., Saubusse, S., Froidefond, J-M., Parlanti, E. 2009. Properties of Fluorescent Dissolved Organic Matter in the Gironde Estuary. Org. Geochem. 40, 706-719. https://doi.org/10.1016/j.orggeochem.2009.03.002.

IBGE, 2018. Instituto Brasileiro de Geografia e Estatistica. https://cidades.ibge.gov.br/brasil/rj/panorama/ (Accessed December 13, 2018).

IPCC (2014). In Climate Change 2014: Synthesis Report. Contribution of Working Groups I, II and III to the Fifth Assessment Report of the Intergovernmental Panel on Climate Change. Editors R. K. Pachauri and L. A. Meyer (Geneva, Switzerland: IPCC).

Jiang, Y., Zhao, J., Li, P., Huang, Q. 2016. Linking optical properties of dissolved organic matter to multiple processes at the coastal plume zone in the East China Sea. Environ. Sci.: Processes Impacts. 18, 1316. https://doi.org/10.1039/c6em00341a.

Lambert, T., Perolo, P., Escoffier, N., Perga, M. E. 2022. Enhanced bioavailability of dissolved organic matter (DOM) in human-disturbed streams in Alpine fluvial networks. Biogeosciences, 19, 187-200. https://doi.org/10.5194/bg-19-187-2022.

Lambert, T., Darchambeau, F., Bouillon, S., Alhou, B., Mbega, J.-D., Teodoru, C.R., Nyoni, F.C., and Borges, A.V.: Landscape control on the spatial and temporal variability of chromophoric dissolved organic matter and dissolved organic carbon in large African rivers. 2015. Ecosystems. 18, 1224–1239. https://doi.org/ 10.1007/s10021-015-9894-5.

Lancelot, C., Muylaert, K. 2011. Trends in estuarine phytoplankton ecology. In: McLusky, D.S., Wolanski, E. (Eds.), Treatise on Estuarine and Coastal Science. Academic Press, Amsterdam, pp. 5–15.

Ludwig, W., Probst, J.L. 1998. River sediment discharge to the oceans: present-day controls and global budgets. Am. J. of Sci. 298, 265–295.

Laws, E.A., Falkowski, P.G., Smith, W.O. Jr, Ducklow, H., McCarthy, J.J. 2000. Temperature effects on export production in the open ocean. Glob. Biogeochem. Cycles. 14, 1231–1246. https://doi.org/10.1029/1999GB001229.

Maher, D.T., Cowley, K., Santos, I.R., Macklin, P., Eyre, B.D. 2015. Methane and carbon dioxide dynamics in a subtropical estuary over a diel cycle: insights from automated in situ radioactive and stable isotope measurements. Mar. Chem. 168, 69–79. https:// doi.org/10.1016/j.marchem.2014.10.017.

Marques, J.S.J., Dittmar, T., Niggemann, J., Almeida, M. G., Gomez-Saez, G. V., Rezende, C.E. 2017. Dissolved Black Carbon in the Headwaters-to-Ocean Continuum of Paraíba Do Sul River, Brazil. Front. Earth Sci., 5, 1–12. https:// doi.org/10.3389/feart.2017.00011.

Massicote, P., Frenette, J-J. 2011. Spatial connectivity in a large river system: resolving the sources and fate of dissolved organic matter. Ecol. Appl. 21(7), 2600-2617. https:// doi.org/10.1890/10-1475.1.

Medeiros, P.M., Seidel, M., Gifford, S.M., Ballantyne, F., Dittmar, T., Whitman, W.B., Moran, M.A. 2017. Microbially-Mediated Transformations of Estuarine Dissolved Organic Matter. Front. Mar. Sci. 4,69. https:// doi.org/10.3389/fmars.2017.00069.

Moran, M. A., Zepp, R. 1997. Role of photoreactions in the formation of biologically labile compounds from dissolved organic matter. Limnol. Oceanogr. 42, 1307–1316. https:// doi.org/10.4319/lo.1997.42.6.1307.

Murphy, K. R., Stedmon, C. A., Graeber, D., Bro, R. 2013. Fluorescence spectroscopy and multi-way techniques, PARAFAC. Anal. Methods. 5, 6557–6566. https:// doi.org/ 10.1039/C3AY41160E.

Ohno, T. 2002. Fluorescence inner-filtering correction for determining the humification index of dissolved organic matter. Environ. Sci. Technol. 36, 742–746. https:// doi.org/ 10.1021/Es0155276.

Osburn, C.L., Boyd, T.J., Montgomery, M.T., Bianchi, T.S., Coffin, R.B., Paerl, H.W. 2016. Optical Proxies for Terrestrial Dissolved Organic Matter in Estuaries and Coastal Waters. Front. Mar. Sci. 2,127. https:// doi.org/ 10.3389/fmars.2015.00127.

Osterholz, H., Kirchman, D.L., Niggemann, J., Dittmar, T. 2016. Environmental Drivers of Dissolved Organic Matter Molecular Composition in the Delaware Estuary. Front. Earth Sci. 4,95. https:// doi.org/10.3389/feart.2016.00095.

Ovalle, A. R. C., Silva, C. F., Rezende, C. E., Gatts, C. E. N., Suzuki, M. S., Figueiredo, R. O. 2013. Long-term trends in hydrochemistry in the Paraíba do Sul River, southeastern Brazil. J. Hydrol. 481, 191–203. https://doi.org/10.1016/j.jhydrol.2012.12.036

Peierls, B.L., Hall, N.S., Paerl, H.W. 2012. Non-monotonic responses of phytoplankton biomass accumulation to hydrologic variability: a comparison of two coastal plain North Carolina estuaries. Estuar. Coasts. 35, 1376–1392. https://doi.org/10.1007/s12237-012-9547-2.

Raymond, P.A., Bauer, J.E. 2000. Bacterial consumption of DOC during transport through a temperate estuary. Aquat. Microb. Ecol. 22,1–12. https://doi.org/ 10.3354/ame022001.

Raymond, P.A., Saiers, J. E.,Sobczak, W. V. 2016. Hydrological and biogeochemical controls on watershed dissolved organic matter transport: pulse- shunt concept. Ecology, 97(1), 5–16. https://doi.org/10.1890/07-1861.1.

Regier, P., Brice-o, H.O., Jaffé, R. 2016. Long-term environmental drivers of DOC fluxes: linkages between management, hydrology and climate in a subtropical coastal estuary. Estuar. Coast. Shelf Sci. 182,112–122. https://doi.org/10.1016/ j.ecss.2016.09.017.

Regier, P., Jaffé, R. 2016. Short-term dissolved organic carbon dynamics reflect tidal, water management, and precipitation patterns in a subtropical estuary. Front. Mar. Sci. 3, 250. https://doi.org/10.3389/fmars.2016.00250.

Rezende, C.E., Lacerda, L.D. Ovalle, A.R.C., Silva, L.F.F. 2007. Dial organic carbon fluctuations in a mangrove tidal creek in Sepetiba bay, Southeast Brazil. Braz. J. Biol. 67, 673-680. https://doi.org/10.1590/S1519-69842007000400012.

Rudorff, N.M., Kampel, M., Rezende, C.E. 2011. Spectral mapping of the Paraıba do Sul River plume (Brazil) using multitemporal Landsat images. J. App. Rem. Sens. 5(1), 053550. https://doi.org/ 10.1117/1.3630220.

Seidel, M., Yager, P.L., Ward, N., Carpenter, E.J., Gomes, H.R., Krusche, A.V., Richey, J.E., Dittmar, T., Medeiros, P.M. 2015. Molecular-level changes of dissolved organic matter along the Amazon River-to-ocean continuum. Mar. Chem. 177(2), 218-231. http://dx.doi.org/10.1016/j.marchem.2015.06.019.

Søndergaard, M., Williams, P.J.L.B., Cauwet, G., Riemann, B., Robinson, C., Terzic, S., Woodward, E.M.S., Worm, J. 2000. Net accumulation and flux of dissolved organic carbon and dissolved organic nitrogen in marine plankton communities. Limnol. Oceanogr. 45, 1097–1111. https://doi.org/10.4319/lo.2000.45.5.1097.

Souza, T. A., Godoy, J. M., Godoy, M.L.D.P., Moreira I., Carvalho Z. L., Salomão, M. S. M. B., Rezende, C. E., 2010. Use of multitracers for the study of water mixing in the Paraíba do Sul River estuary. J. Environ. Radioact. 101, 564–570. https://doi.org/ 10.1016/j.jenvrad.2009.11.001.

Sterza, J. M., Fernandes, L. L. 2006. Distribution and abundance of cladocera (brachiopoda) in the Paraiba do Sul River Estuary, Rio de Janeiro, Brazil. Braz. J. Oceanogr. 54, 193-204 https://doi.org/10.1590/S1679-87592006000300003.

Stedmon, C. A., Bro, R. 2008. Characterizing dissolved organic matter fluorescence with parallel factor analysis: a tutorial. Limnol. Oceanogr. Meth. 6, 572–579. https://doi.org/10.4319/lom.2008.6.572.

Stedmon, C. A., Thomas, D.N., Granskog, M., Kaartokallio, H., Papadimitriou, S., Kuosa, H. 2007. Characteristics of Dissolved Organic Matter in Baltic Coastal Sea Ice: Allochthonous or Autochthonous Origins? Environ. Sci. Technol. 41(21), 7273-7279. https://doi.org/10.1021/es071210f.

Stedmon, C.A., Markager, S. 2005. Resolving the variability in dissolved organic matter fluorescence in a temperate estuary and its catchment using PARAFAC analysis. Limnol. Oceanogr. 50(2), 686-697. https://doi.org/10.4319/lo.2005.50.2.0686.

Strickland, J.D.H., Parsons, T.R. 1972. A Practical Handbook of Seawater Analysis. Fisheries Research Board of Canada Bulletin, Ottawa.

Yamashita, Y., Jaffe, R., Maie, N., Tanoue, E. 2008. Assessing the dynamics of dissolved organic matter (DOM) in coastal environments by excitation and emission matrix fluorescence and parallel factor analysis (EEM-PARAFAC), Limnol. Oceanogr., 53, 1900–1908. https://doi.org/10.4319/lo.2008.53.5.1900

Yang, L., Cheng, Q., Zhuang, W-E, Wang, H., Chen, W. 2019. Seasonal changes in the chemical composition and reactivity of dissolved organic matter at the land-ocean

interface of a subtropical river. Environ Sci. Pollut. Res. 26, 24595–24608. https://doi.org/10.1007/s11356-019-05700-2.

Yang, L., Hong, H., Chen, C-T. A., Guo, W., Huang, T-H. 2013. Chromophoric dissolved organic matter in the estuaries of populated and mountainous Taiwan. Mar. Chem. 157, 12-23. https://doi.org/10.1016/j.marchem.2013.07.002.

Zepp, R. G., Sheldon, W. M., Moran, M. A. 2004. Dissolved organic fluorophores in southeastern US coastal waters: correction method for eliminating Rayleigh and Raman scattering peaks in excitation–emission matrices. Mar. Chem., 89, 15–36, https://doi.org/10.1016/j.marchem.2004.02.006.

Ziervogel, K., Osburn, C., Brym, A., Battles, J., Joye, S., D'souza, N., Montoya, J., Passow, U., Arnosti, C. 2016. Linking heterotrophic microbial activities with particle characteristics in waters of the Mississippi River delta in the Aftermath of Hurricane Isaac. Front. Mar. Sci. 3:8. https://doi.org/10.3389/fmars.2016.00008.

Walker, S. A., Amon, R. M. W., Stedmon, C., Duan, S., Louchouarn, P. 2009. The use of PARAFAC modeling to trace terrestrial dissolved organic matter and fingerprint water masses in coastal Canadian Arctic surface waters. J. Geophys. Res. 114, G00F06, https://doi.org/10.1029/2009JG000990.

Figure Captions

Table 1. Discharge, mean (±standard deviation), minimum and maximum values of the principal physicochemical properties of the waters separated by sampling campaigns.

Table 2. Mean and standard deviation for DOC (mg L^{-1}) for CDOM and FDOM indices: SR, a350 (m^{-1}) and HIX and component contributions (F_{max} and %), separated by sampling campaigns and estuarine zone.

Table 3. Spectral properties (positions of maximum excitation (ex) and emission (em) peaks) of the six PARARAC components identified in this study, general description and dominant sources based on previous studies.

Figure 1. Map 1a shows the localization of the Rio the Janeiro State. Map 1b shows the localized PSRE and adjacent shelf waters. The orange line represents the boat's track. The blue squares represent the locations of the stations. The red triangle represents the localization of the anchored station (Eulerian time series). Panel c shows a comparison

between the river water discharge for the year of sampling (2017/2018) and the historical average. The red arrows are the sampled months. Panel d shows a historical tendency of decreasing river flow (monthly averaged values).

Figure 2. Comparison of DOC (mg L^{-1}), S^R, a_{350} (m^{-1}) and HIX values along salinity gradients for the Feb.-17, Oct.-17 and Mar.-18 campaigns.

Figure 3. Six split-half validated fluorescent components calculated from the PARAFAC model on DOM EEMs from the Paraiba do Sul River Estuary (PSRE). Each EEM was normalized to its maximum fluorescence prior to modeling. The solid lines represent the excitation, and the dashed lines represent the emission intensities (nm).

Figure 4. PCA biplot, including loadings plot for the input variables and scores plot for stations. Markers are shaped according to the sampling temporal and spatial variability of DOM composition and colored according to a gradient salinity and sampling periods. Graphical representation of PCA results for the input variables and scores plot for water samples: **(A)** spatial: mangrove (gray circles), mixing zone (triangles), ocean (squares), river (circles) DOM driven parameters. The optical properties of DOM, including the level of CDOM (a_{350}, S_R, HIX), the relative abundance of PARAFAC components and DOC, Chl *a* salinity, PO_4^- and DIN were used as the variables and **(B)** collected during the Feb.-17 campaign (circles), Oct.-17 campaign (triangles) and Mar.-18 (squares) to explore DOM seasonality.

Figure 5. Relative contribution of PARAFAC components during the different campaigns. All samples have been included here.

Figure 6. FDOM component (F_{max}) diel variability sampling in relation to salinity dissolved organic carbon (DOC) and tidal level conducted in the mangrove tidal creek located in the secondary channel in Mar.- 18 every 3 hours of interval.

CRediT authorship contribution statement

Luciana O Vidal: Conceptualization, Supervision, Investigation, Methodology, Validation, Writing – original draft, Writing – review & editing, Formal analysis, Data curation, Visualization. **Thibault Lambert:** Writing – original draft, Writing – review & editing, Formal analysis, Data curation, Visualization, Methodology, Validation. **Luiz Cotovicz Jr.:** Investigation, Writing – original draft, Writing – review & editing, Formal analysis, Data curation, Visualization. **Marcelo C. Bernardes:** Writing – review & editing. **Rodrigo Sobrinho:** Writing – review & editing. **Fabiano Thompson:** Writing – review & editing. **Gisele D. Garcia:** Writing – review & editing. **Bastian A. Knoppers:** Writing – review & editing. **Pedro V. Gatts:** Data curation; Writing – review & editing. **Carolina R. Régis:** Data curation; Writing – review & editing. **Gwenaël Abril:** Writing – review & editing. **Carlos E. de Rezende:** Conceptualization, Investigation, Resources, Writing – review & editing, Visualization, Supervision, Project administration.

Declaration of interests

☒The authors declare that they have no known competing financial interests or personal relationships that could have appeared to influence the work reported in this paper.

☐The authors declare the following financial interests/personal relationships which may be considered as potential competing interests:

Fig. 1

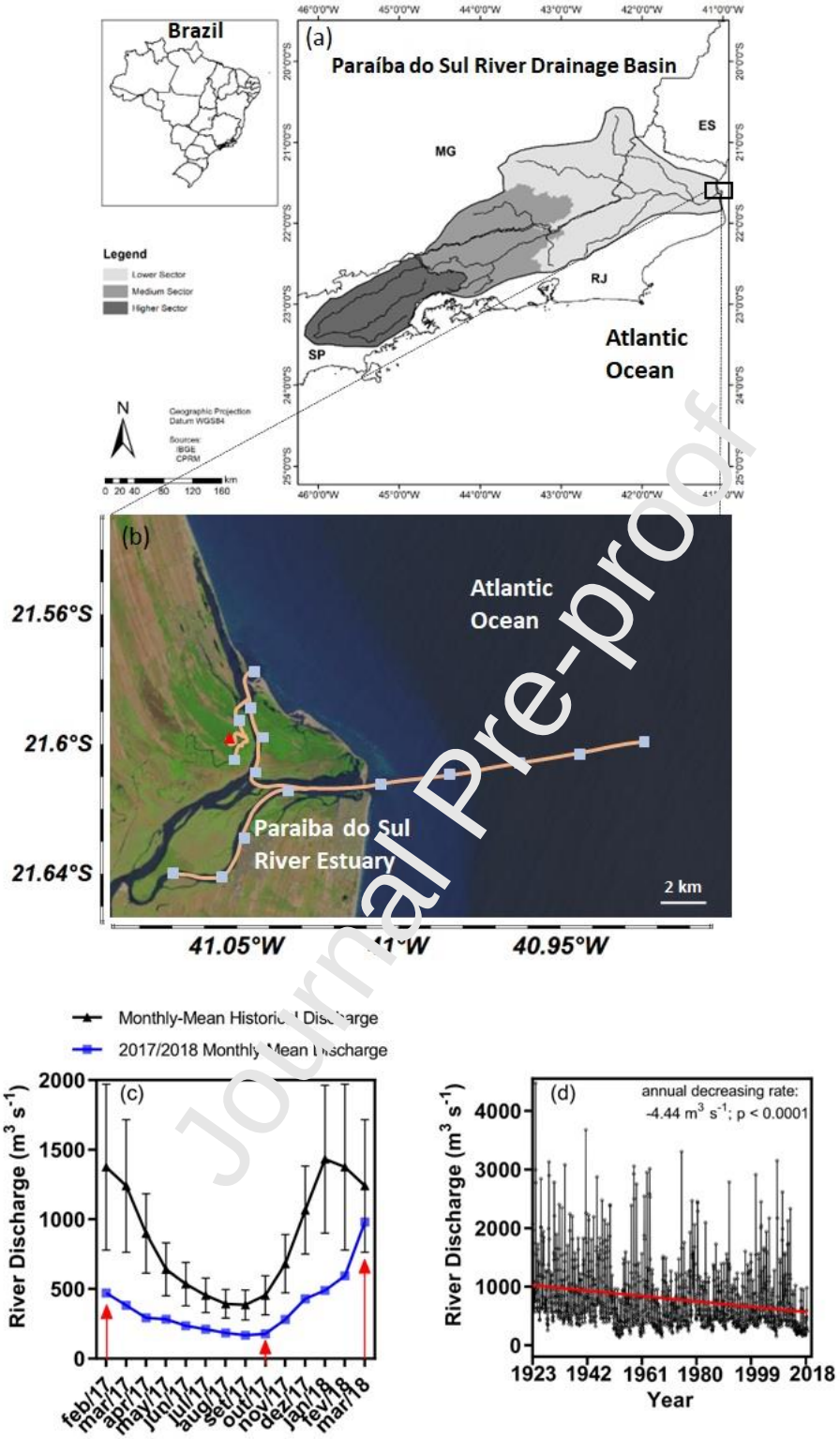

Fig. 2

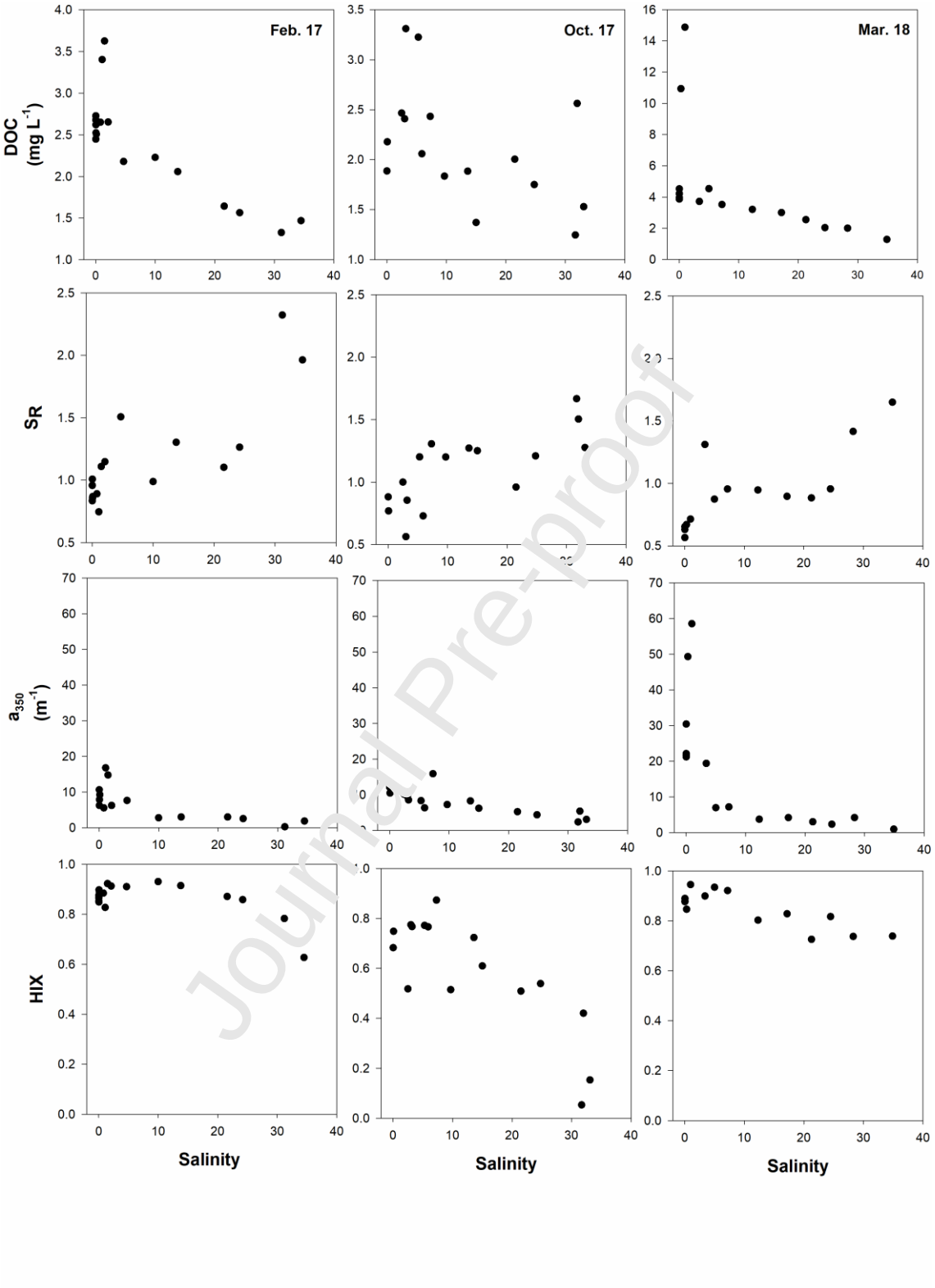

Fig. 3

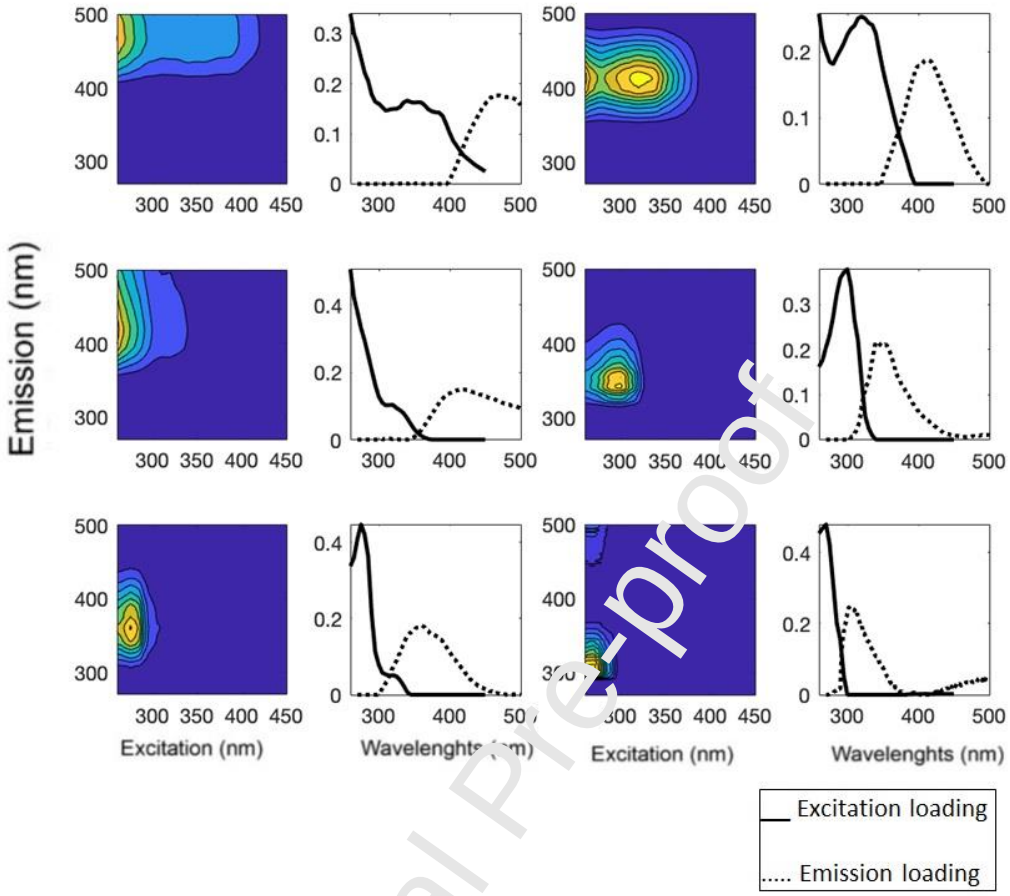

Fig. 4

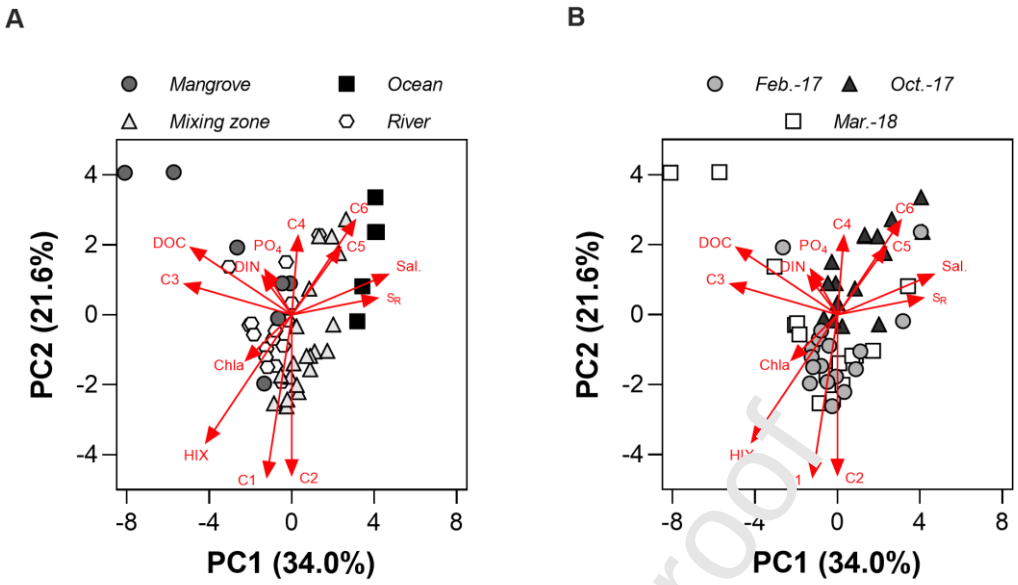

Fig. 5

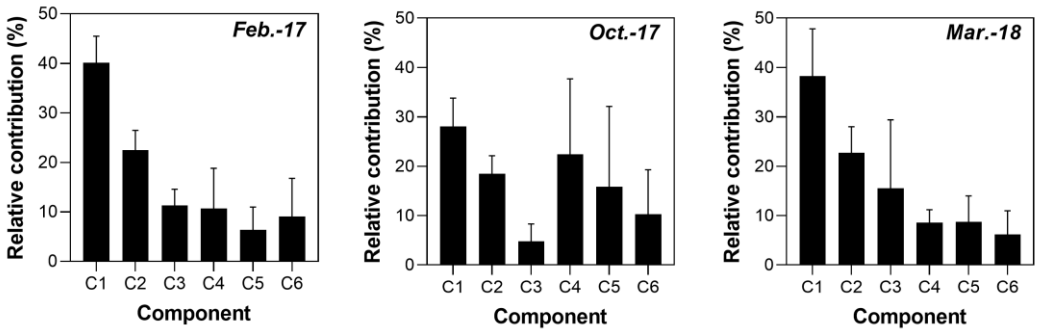

Fig. 6

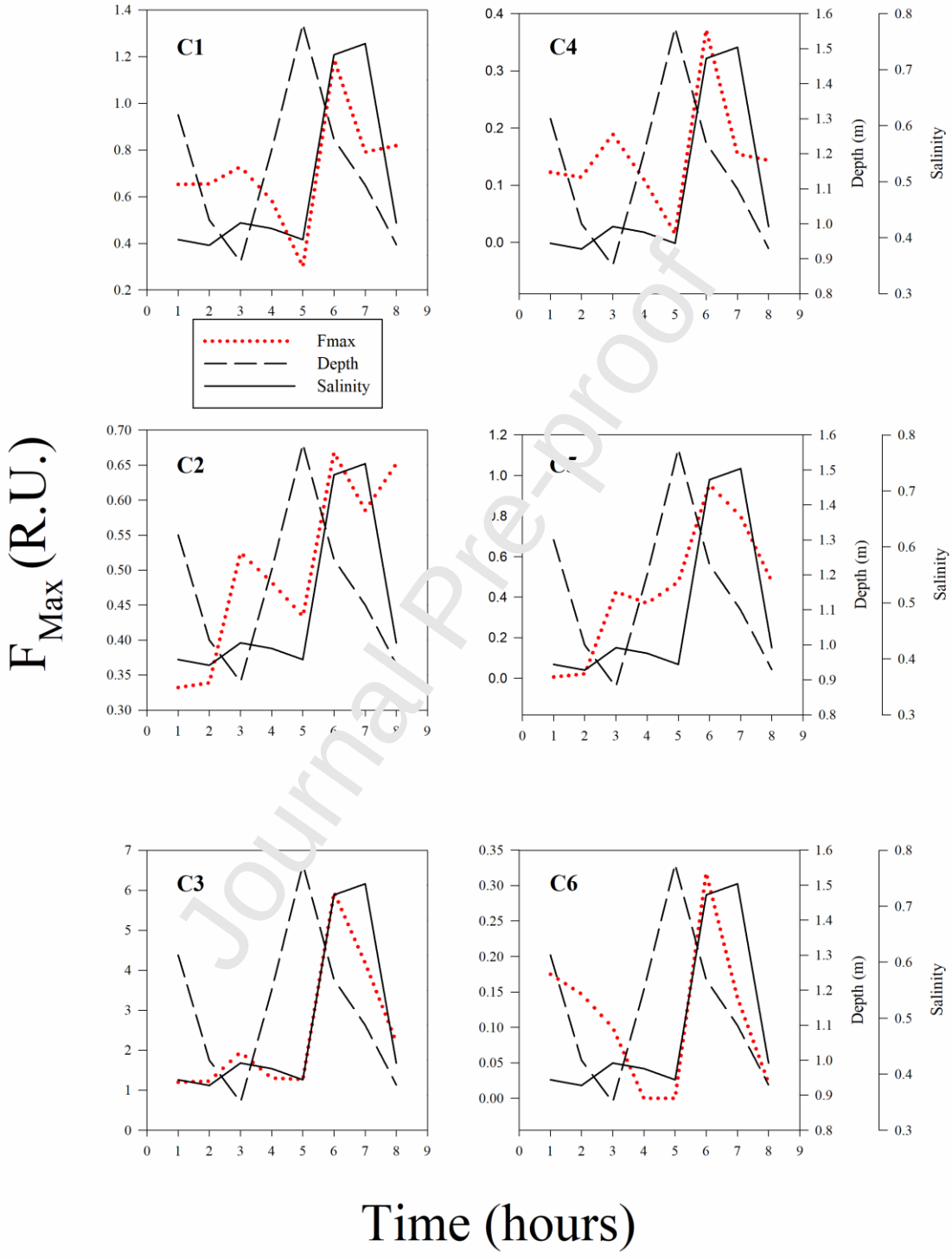

Table 1 - Discharge, mean (±standard deviation), minimum and maximum values of the principal physicochemical
properties on the waters separated by sampling campaigns.

Estuarine sampling	Discharge ($m^3 s^{-1}$)	Sal.	Temp. (°C)	SPM (mg L^{-1})	Chl *a* (µg L^{-1})
Feb. – 17 first dry (n = 17)	288	8.58 ± 11.95 (0.03 / 34.5)	28.63 ± 1.33 (26.2 / 31.14)	9.93 ± 4.37 (3.14/ 16.55)	10.52 ± 6.71 (0.00/ 23.55)
Oct. – 17 second dry (n = 16)	178	13.04 ± 11.9 (0.04 / 33.1)	25.2 ± 0.74 (23.5 / 25.9)	23.44 ± 34.22 (3.76 / 147,85)	1.46 ± 3.5 (0.00 / 14.28)
Mar. – 18 wet (n = 15)	1,240	10.36 ± 11.9 (0.03 / 34.9)	29.38 ± 1.08 (27.9 / 31.6)	22.94 ± 16.2 (4.05 / 49.41)	1.53 ± 2.09 (0.03 / 7.12)

Table 2: Mean and standard deviation for DOC (mg L^{-1}), for CDOM and FDOM indexes: SR, a350 (m^{-1}) and HIX and components contribution (Fmax and %), separated by sampling campaigns and estuarine zone.

Campaign	Site	DOC (mg L^{-1})	S_R	a_{350} m^{-1}	HIX	FMax (R.U.)						%C					
						C1	C2	C3	C4	C5	C6	C1	C2	C3	C4	C5	C6
Feb.-17	River	2.60 ± 0.10	0.94 ± 0.10	8.35 ± 2.18	0.88 ± 0.22	0.42 ± 0.04	0.23 ± 0.01	0.13 ± 0.02	0.10 ± 0.03	0.08 ± 0.05	0.08 ± 0.03	40.23 ± 2.13	22.27 ± 2.05	12.77 ± 1.67	9.26 ± 1.54	7.60 ± 4.06	7.85 ± 2.22
	Mangrove	3.51 ± 0.16	0.93 ± 0.26	15.75 ± 1.42	0.87 ± 0.07	0.53 ± 0.05	0.32 ± 0.05	0.17 ± 0.01	0.29 ± 0.41	0.04 ± 0.05	0.03 ± 0.001	36.89 ±9.88	22.23 ± 7.36	11.73 ± 2.78	24.44 ± 24.01	2.64 ± 3.73	2.06 ± 0.25
	Mixing zone	1.93 ± 0.31	1.23 ± 0.20	3.78 ± 2.15	0.90 ± 0.03	0.25 ± 0.10	0.14 ± 0.06	0.06 ± 0.03	0.04 ± 0.02	0.03 ± 0.02	0.03 ± 0.01	44.29 ±2.73	25.37 ± 2.35	11.49 ± 1.21	7.38 ± 0.80	4.98 ± 1.48	6.48 ± 3.62
	Ocean	1.40 ± 0.10	2.14 ± 0.25	1.04 ± 1.14	0.70 ± 0.11	0.04 ± 0.02	0.02 ± 0.01	0.001 ± 0.006	0.01 ± 0.00	0.009 ± 0.01	0.03 ± 0.00	32.64 ±9.16	16.23 ± 5.63	4.35 ± 4.67	10.64 ± 2.16	8.59± 11.67	27.54 ± 5.62
Oct.-17	River	2.23 ± 0.26	0.80 ± 0.19	10.51 ± 1.08	0.68 ± 0.12	0.25 ± 0.03	0.16 ± 0.02	0.03 ± 0.02	0.19 ± 0.19	0.18 ± 0.20	0.07 ± 0.02	29.14 ±5.07	18.53 ± 4.13	4.01 ± 1.81	20.32 ± 16.16	20.32 ± 22.18	7.67 ± 1.60
	Mangrove	2.99 ± 0.48	1.12 ± 0.24	10.88 ± 4.29	0.80 ± 0.06	0.43 ± 0.24	0.24 ± 0.11	0.12 ± 0.09	0.40 ± 0.02	0.03 ± 0.03	0.04 ± 0.02	32.63 ±4.85	18.86 ± 1.48	8.73 ± 3.26	35.09 ± 11.88	1.89 ± 1.78	2.79 ± 1.24
	Mixing zone	1.92 ± 0.36	1.16 ± 0.25	6.11 ± 1.30	0.58 ± 0.12	0.17 ± 0.05	0.12 ± 0.04	0.03 ± 0.03	0.14 ± 0.19	0.12 ± 0.14	0.07 ± 0.04	27.31 ±6.03	18.97 ± 4.48	3.40 ± 3.88	21.69 ± 16.40	17.22 ± 15.32	10.80 ± 5.73

	Ocean	1.39 ± 0.20	1.47 ± 0.28	2.68 ± 0.51	0.10 ± 0.07	0.08 ± 0.03	0.06 ± 0.02	0.01 ± 0.003	0.04 ± 0.03	0.07 ± 0.03	0.11 ± 0.11	22.16 ±2.02	16.63 ± 2.38	3.30 ± 0.60	10.20 ± 3.33	23.02 ± 17.92	24.67 ± 19.60
Mar.-18	River	4.14 ± 0.30	0.63 ± 0.04	23.84 ± 4.39	0.88 ± 0.01	0.81 ± 0.15	0.47 ± 0.01	0.43 ± 0.21	0.23 ± 0.02	0.13 ± 0.10	0.15 ± 0.04	36.89 ±8.11	21.24 ± 1.30	19.09 ± 8.42	10.27 ± 1.09	5.80 ± 4.01	6.70 ± 1.80
	Mangrove	12.91 ± 2.78	0.69 ± 0.03	53.89 ± 6.51	0.89 ± 0.07	1.43 ± 0.27	0.76 ± 0.34	2.84 ± 1.08	0.49 ± 0.27	0.30 ± 0.42	0.44 ± 0.50	32.82 ±0.58	11.87 ± 2.82	44.55 ± 7.73	8.50 ± 6.12	4.22 ± 5.83	8.06 ± 9.66
	Mixing zone	3.07 ± 0.87	1.03 ± 0.21	6.33 ± 5.53	0.83 ± 0.08	0.40 ± 0.23	0.23 ± 0.13	0.07 ± 0.02	0.06 ± 0.22	0.08 ± 0.47	0.03 ± 0.013	44.43 ±3.97	26.40 ± 1.98	8.37 ± 2.60	7.47 ± 1.75	9.42 ± 2.23	3.92 ± 1.49
	Ocean	1.28	1.65	0.92	0.74	0.04	0.03	0.00	0.02	0.04	0.03	25.73	20.64	0.44	11.60	22.74	18.86

Table 3 – Spectral properties (positions of maximum excitation (ex) and emission (em) peaks) of the six PARARAC components identified in this study, general description and dominant sources based on previous studies.

Component	Max ex (nm)	Max em (nm)	Description & dominant source
C1	260(340)	464	Fulvic-acid like fluorophore, widespread, terrestrial origin[a].
C2	260(320)	412	Humic-like fluorophore, widespread, terresstrial origin[b].
C3	260(320)	418	Humic-like fluorophore, terrestrial origin[c], indicative of wetland/floodplains origin[d].
C4	280(300)	340	Protein-like fluorophore, indicative of bacterial degradation[b].
C5	280(320)	360	Tryptophan-like fluorophore, indicative of autochthonous production[e].
C6	270(290)	302	Tyrosine-like fluorophore, indicative of autochthounous production[f].

(a)Osburn et al., 2016; (b)Asmala et al., 2018; (c)Stedmon and Markager, 2005; (d)Stedmon et al., 2007; Massicote and (e)Frenette, 2011; (f)Walker et al., 2009

Graphical abstract

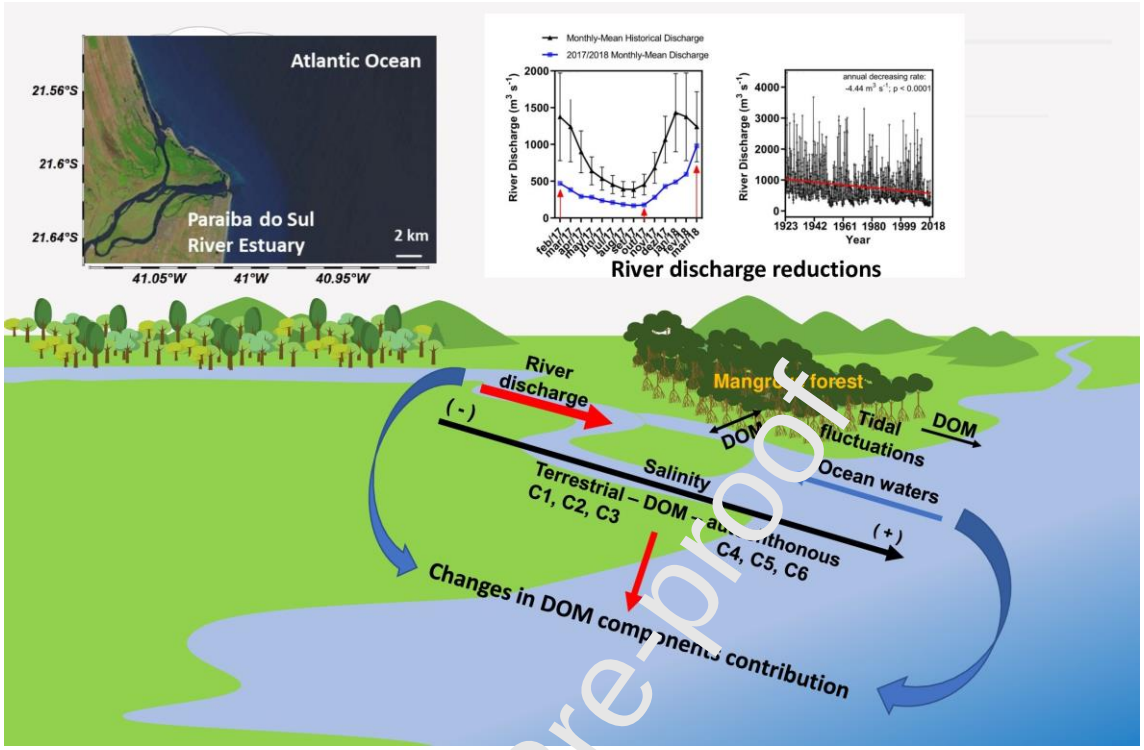

HIGHLIGHTS

- CDOM and FDOM across an estuarine salinity gradient under three river discharge conditions were studied;
- Six DOM components across the river-ocean gradient and mangrove creek were identified;
- DOM allochthonous-authochonous components showed similar contribution during high and low discharges;
- The combination of lower river discharge level and tide influenced DOM components contribution across the river-ocean gradient;
- High river discharge showed the highest terrestrial DOM transport to the ocean;
- Mangrove terrestrial carbon showed to be tidal modulated and contributed to estuarine DOM.